JOURNAL OF MATERIALS SCIENCE 16 (1981) 125–140

A double torsion fracture mechanics and Auger electron spectroscopy approach to the study of stress corrosion cracking in low alloy steels

A. BRIGGS*, R. AIREY*, B. C. EDWARDS‡
*Materials Development** *and Metallurgy‡ Divisions, AERE Harwell, Oxon, UK*

The applicability of the double torsion fracture mechanics test to the study of stress corrosion cracking (SCC) in steels was assessed by evaluating the behaviour of the low alloy steels AISI 4140 and En30A, exhibiting both high (1400 MNm^{-2}) and low (765 MNm^{-2}) yield strengths respectively. An optical method for measuring crack growth rate and a load relaxation method for computing it were compared and found to give similar results. The test was shown to be eminently suitable for the study of SCC in high yield strength steels and those in a temper embrittled condition. The influence of trace impurities on the SCC susceptibility was examined using Auger electron spectroscopy to determine the type and amount of grain boundary segregants. The degree of segregation of trace impurities was shown to have a profound effect on the stress intensity–crack velocity ($K-V$) diagram by reducing K_{IC} and increasing the reaction rate as shown by the increased slope in stage III of the $K-V$ diagram. An anomalously low threshold stress intensity was observed in as-quenched AISI 4140 and this was attributed to residual stresses produced by the phase transformations occurring during quenching.

1. Introduction

The nucleation and sub-critical growth of cracks under the combined influence of stress and chemical attack, defined as stress corrosion cracking (SCC), has been observed in a wide variety of metallic and non-metallic materials [1–5]. This phenomenon is a potentially serious problem in many alloys [6], and particularly in low alloy, high strength steels in aqueous environments. It is known that hydrogen can be generated at a steel surface, especially if the latter is freshly exposed, by a corrosion reaction with water [7, 8]. At the tip of a growing crack, where the conditions (stress intensity; continual exposure of fresh surface) are particularly favourable for the generation and absorption of hydrogen, they also favour further growth of the crack, which can lead to a critical situation. The corrosion reaction at or near a crack tip may be cathodic or anodic and may lead to crack growth by hydrogen embrittlement (hydrogen-assisted cracking) or active path corrosion respectively [9, 10]. Which of the reactions is the more important in a particular case can be determined by electrochemical polarization experiments [9–11]. It is now reasonably well established that the mechanism of SCC in high strength steels involves hydrogen-assisted cracking [12–17].

A useful approach to the study of stress corrosion cracking is that of fracture mechanics, in which the growth rate of a crack is related to the stress intensity at its tip. The validity of this approach has been demonstrated by Brown [18], who assessed a wide variety of specimen geometries, crack opening modes and stressing methods. One important fracture mechanics test which was not discussed by Brown is the double torsion test, developed by Outwater *et al.* [19] and extended by Evans and Williams [20–22] for the study of ceramic materials. Advantages of this test are:

0022–2461/81/010125–16$03.60/0

specimens are easily machined and therefore inexpensive; only small-scale specimens and testing machines are required, even for the study of the effects of long cracks; for a given load the crack tip stress intensity is the same, irrespective of the crack length [23] and in principle a complete stress intensity–crack velocity diagram can be obtained from a single specimen. This test method has been little used to study the fracture mechanics of steels. Williams and Evans [21] examined its application to AISI 4340 steel as part of an experimental survey of the validity of the test as a universal one for a variety of materials, but the only comprehensive double torsion test work reported for steel is that of Brunton [24] who used an optical crack-monitoring technique to produce stress intensity–crack velocity ($K-V$) diagrams for AISI 4140 steel after various heat treatments and in various environments.

The main objectives of the present study were: (i) to assess the validity of the double torsion test for low alloy steels, AISI 4140 and En30A, exhibiting both high ($\sim 1400\,MNm^{-2}$) and low ($765\,MNm^{-2}$) yield strengths respectively, (ii) to compare the results obtained using Brunton's crack velocity measuring method [24] with those obtained using the less laborious load relaxation variant of the double torsion test developed by Evans [20], and (iii) to investigate the effects of grain boundary segregation on the SCC susceptibility.

Recent work by McMahon and co-workers [25, 26] has shown that the threshold stress intensity, K_{th}, for hydrogen-assisted cracking in gaseous hydrogen is a sensitive function of the grain boundary composition. Very little information exists on the effects of trace impurities on the SCC behaviour, but K_{th} in 4340 steel has been shown [17] to be independent of the prior austenite grain size but dependent upon the C and Mn levels.

In the present work the SCC susceptibility of AISI 4140 steel in the as-quenched and quenched and tempered state, and the En30A steel in a temper embrittled and unembrittled condition has been studied. The SCC behaviour in relation to the degree of segregation of trace elements to the grain boundaries was investigated using Auger electron spectroscopy (AES).

2. Theoretical considerations

The relationship between stress intensity at the tip of a crack and the rate of growth of the crack may be described completely by a stress intensity–crack velocity ($K-V$) diagram. Fig. 1 shows, schematically, the typical features of such a diagram. Stage I is believed to be reaction rate controlled, whilst stage II is controlled by the rate of diffusion of hydrogen, produced by the reaction, into the material ahead of the crack tip. This second stage may, in some circumstances, be insensitive to the stress intensity, resulting in a plateau on the diagram. In stage III, K_I is close to the critical stress intensity, K_{IC}, and crack propagation is due to a combination of corrosive and mechanical failure. The stress intensity, K_I, depends only upon the load and the specimen geometry and, for the case of the double torsion test, has been shown by Kies and Clark [23] to be independent of crack length. Then

$$K_I = AP \qquad (1)$$

where P is the applied load and A is a constant which depends on the specimen dimensions. A can be derived through the analysis of Keis and Clark [23] or obtained experimentally by means of an independent determination of K_{IC}, the critical stress intensity [5], when

$$K_{IC} = AP_c$$

where P_c is the critical load.

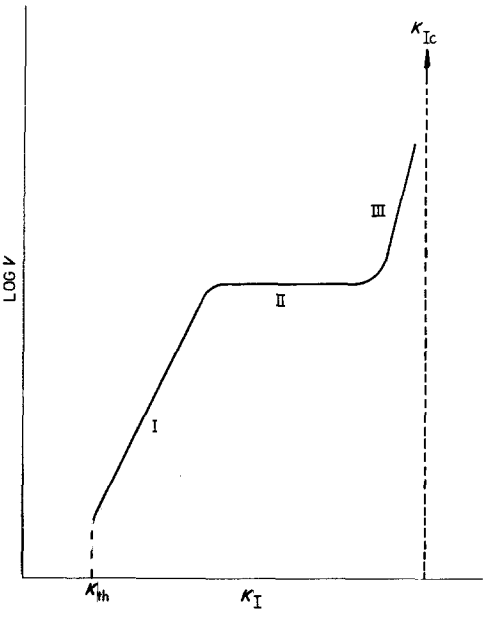

Figure 1 Schematic representation of the dependence of crack velocity, V, on stress intensity, K_I. ($K-V$ diagram).

For the application of the double torsion technique to a material to be valid, it must be shown that the displacement at the loading point, y, is linearly related to the crack length, a, so that the compliance,

$$\frac{y}{P} = Ba + C \tag{2}$$

where B and C are constants which can be derived from a compliance calibration. The validity of the test having been established, and K_I determined, average crack velocities for various constant loads may be obtained from optical measurements of crack length.

A less laborious approach is the load relaxation method developed by Evans [20], the theoretical basis of which is as follows. Rearrangement of Equation 2 and differentiation with respect to time gives

$$\frac{dy}{dt} = (Ba + C)\frac{dP}{dt} + BP\frac{da}{dt} \tag{3}$$

where $(da/dt) = V$, the crack velocity. At constant displacement, $(dy/dt) = 0$ and therefore,

$$\frac{da}{dt} = -\frac{(Ba + C)}{BP}\frac{dP}{dt}. \tag{4}$$

Also, at constant displacement, y

$$P(Ba + C) = P_i(Ba_i + C)$$

where a_i is the initial crack length and P_i the initial load at the start of relaxation. Substituting for a in Equation 4 gives

$$\frac{da}{dt} = -\frac{P_i}{P^2}\left(a_i + \frac{C}{B}\frac{dP}{dt}\right). \tag{5}$$

For $a_i \gg (c/B)$ Equation 5 reduces to

$$\frac{da}{dt} = -\frac{a_i P_i}{P^2}\frac{dP}{dt}. \tag{6}$$

The crack velocity can thus be obtained directly from the rate of load relaxation at constant displacement and the initial crack length, a range of velocities being obtainable from a single relaxation curve.

In the present work the optical crack measurement and load relaxation approaches have been compared, to determine their relative usefulness in double torsion stress corrosion testing of low alloy steels.

TABLE I Compositions of the AISI 4140 and En30A steels studied

Element	AISI 4140 (wt %)	En30A (wt %)
Ni	0.23	4.06
Cr	1.08	1.20
Mn	1.00	0.58
Mo	0.14	0.11
Si	0.16	0.32
C	0.39	0.28
P	0.021	0.013
S	–	0.008
Sb	–	0.004
Sn	–	0.014
As	–	0.024
N	–	0.010

3. Experimental procedure

3.1. Materials and heat treatment

Experiments were carried out on two commercial, low alloy steels, AISI 4140 and En30A, whose chemical compositions are given in Table I. The AISI 4140 was machined before heat treatment to give plate specimens 200 mm × 100 mm × 8 mm, each with a central V-groove 0.8 mm deep, cut lengthwise in one face to serve as a crack guide. At one end of the groove a crack starter-notch 10 mm long was machined. In the case of the En30A, plate specimens 200 mm × 100 mm were again prepared, but the thickness was limited to 5 mm by the thickness of plate available, and the V-groove was made correspondingly shallower, 0.5 mm. Fig. 2 is a schematic diagram showing specimen and loading geometries.

The applicability of the test to high strength steels was assessed by examining the behaviour of AISI 4140 low alloy steel in the as-quenched martensitic state and after subjecting the as-quenched material to a 1 h temper at 250° C, the latter treatment being known to promote an increase in the yield stress [27]. The application to lower strength steels was assessed by examining an En30A steel in a temper embrittled and unembrittled state (Table II).

3.2. Compliance calibration

To establish the validity of the double torsion test approach to the study of stress corrosion cracking in steels it was first necessary to carry out a compliance calibration, as follows.

A crack, introduced into a specimen by immersing it in distilled water and applying a 500 kg load, was grown into the central region of the specimen by stress corrosion. The distilled water

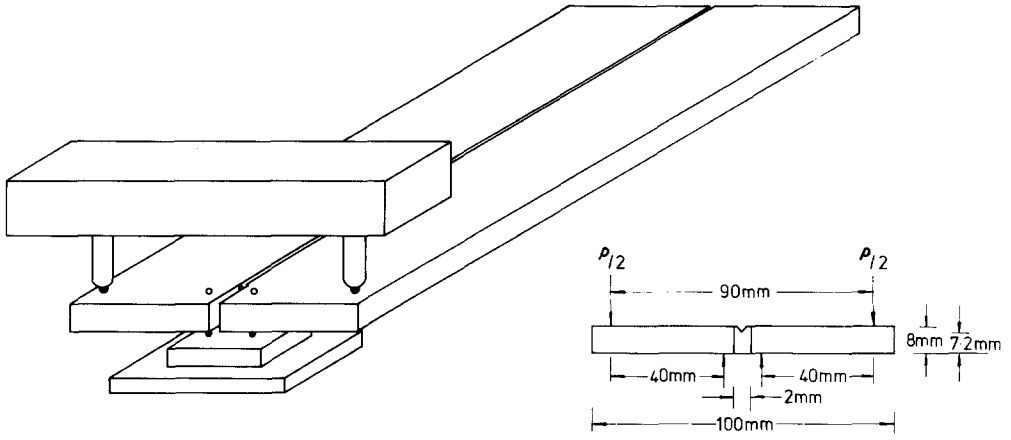

Figure 2 Diagrammatic representation of the loading jig and the double torsion test sample geometry.

was drained, the load removed, the length of the crack measured, and the specimen deflection recorded on application of a 500 kg load. Further crack growth was then induced under stress corrosion conditions, and again the specimen deflection under a 500 kg load recorded. This procedure was repeated for progressively increased crack lengths, to give the compliance calibration curve shown in Fig. 3, which demonstrates the validity of the test for crack lengths less than about 180 mm. From Fig. 3 the constants B and C for Equation 2 are 1.2×10^{-6} N^{-1} and 1.0×10^{-7} mN^{-1} respectively. Since C/B is of the same order as a_i, Equation 6 is not valid, and Equation 5 applies.

3.3. Crack velocity measurement by an optical technique

In the central region of the grooved face of each specimen a 100 mm scale, with 100 μm divisions, was printed by a photo-resist method. The printing was arranged so that the scale appeared on the sides of the groove and on the specimen face adjacent to the groove. By means of an optical stereo-microscope mounted on the testing machine, the scale, and a crack travelling along it, could be observed during a test, with the position of the crack tip measured to an accuracy of $\pm$ 50 μm. To eliminate possible end effects, measurements were taken only when the crack tip was in the central 100 mm of the specimen. The crack was grown initially into this region from the starting notch by application of an appropriate load with the specimen immersed in distilled water to give stress corrosion conditions. The load required to give a suitable crack growth rate was 500 kg for AISI 4140 and 1000 kg for En30A. Each of these loads produced a crack-tip stress intensity approximately two thirds of the critical value, determined in the absence of stress corrosion. When a crack extending onto the scale had been produced, experiments involving the application of constant loads for appropriate times were begun, and the position of the crack measured after each load application. To obtain crack velocity–stress intensity curves the load was varied from $\sim$ 90% of the critical value down to a threshold value at which no crack growth could be detected in 100 h.

Experiments on AISI 4140 were carried out with specimens immersed in distilled water at room temperature or in air at ambient temperature and relative humidity. En30A in the embrittled condition was tested in distilled water at 20 or 80° C. The unembrittled state was tested at 20° C.

TABLE II Heat treatment schedule

Steel	Condition	Heat treatment
AISI 4140	As-quenched	1 h, 850° C, O.Q.*
AISI 4140	Tempered	1 h, 850° C, O.Q. + 1 h, 250° C
En30A	Unembrittled	1 h, 950° C, O.Q. + 1 h, 650° C → W.Q.†
En30A	Temper-embrittled	1 h, 950° C, O.Q. + 1 h, 650° C → W.Q. + 24 h, 500° C

*O.Q. – Oil quench.
†W.Q. – Water quench.

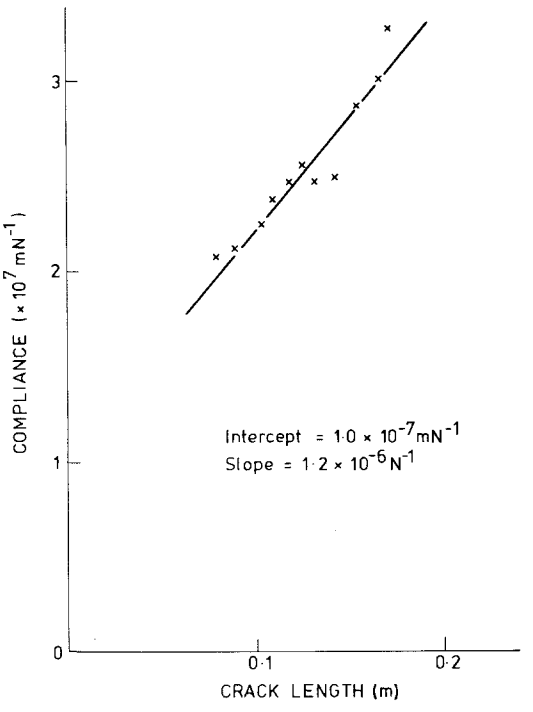

Figure 3 Compliance calibration curve used for the double torsion test piece.

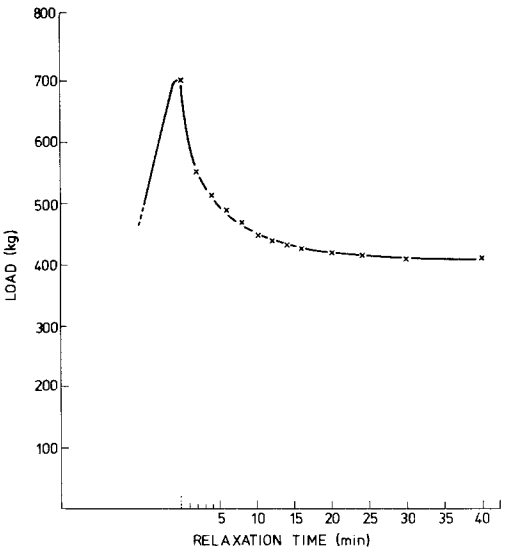

Figure 4 A typical load–relaxation curve obtained using the double torsion test piece.

3.4. Crack velocity by the load relaxation technique

A crack was introduced into the specimen by the method described above, grown until it reached the printed scale in the central region, and its length noted. An initial load was then applied, at a rate of $\sim 250\,\mathrm{kg\,sec^{-1}}$, by hand-operation of the Instron crosshead. The crosshead was stopped and, at constant displacement, the load relaxation recorded; a typical relaxation curve is shown in Fig. 4.

3.5. Auger electron spectroscopy

It is well established that the intergranular failure of low alloy steels may be promoted by the presence of certain trace impurities which segregate to the grain boundaries when the material is subjected to certain heat treatments. This segregation reduces the cohesive strength of the grain boundaries and one manifestation of this phenomenon is that of temper embrittlement in which an increase in the ductile–brittle transition temperature is produced together with a change in the brittle fracture mode from cleavage to intergranular. The presence of such segregation at the grain boundaries has been shown to enhance the susceptibility to hydrogen assisted cracking [25, 26] and liquid metal embrittlement [28]. In the present work the dependence of the SCC susceptibility on the grain boundary composition has been studied using AES to determine the amount and type of grain boundary segregants.

In situ impact fracture of the samples was performed in the HBA 200 Auger system at pressures of about 10^{-10} torr and at -160° C, using the Harwell impact stage [29]. The resulting fracture surfaces were analysed using a hemi-cylindrical mirror analyser with an integral electron gun providing a spot size on the sample of $\sim 4\,\mu$m. The differential energy spectra were recorded at a modulation of 3 V peak to peak, a primary energy of 2.5 keV and a specimen current of $4\,\mu$A. A secondary electron image was used to position the beam on the fracture surface and spectra were recorded systematically across the fracture surface.

Argon ion bombardment (at 3 keV) and subsequent AES analyses were used to progressively remove the surface layers on the specimen and to record the compositional profiles of the segregated species as a function of distance from the "as-fractured" surface. The sample was subsequently re-examined at higher resolution, in a Philips PSEM 500 scanning electron microscope.

To a first approximation, the amplitude of an Auger peak in the $(\mathrm{d}N(E)/\mathrm{d}E)$ spectrum is proportional to the atomic concentration of the element producing that peak [30]. Quantification of the spectra was achieved by expressing the peak height as a percentage of the dominant matrix peak height (namely the Fe 703 eV) and converting

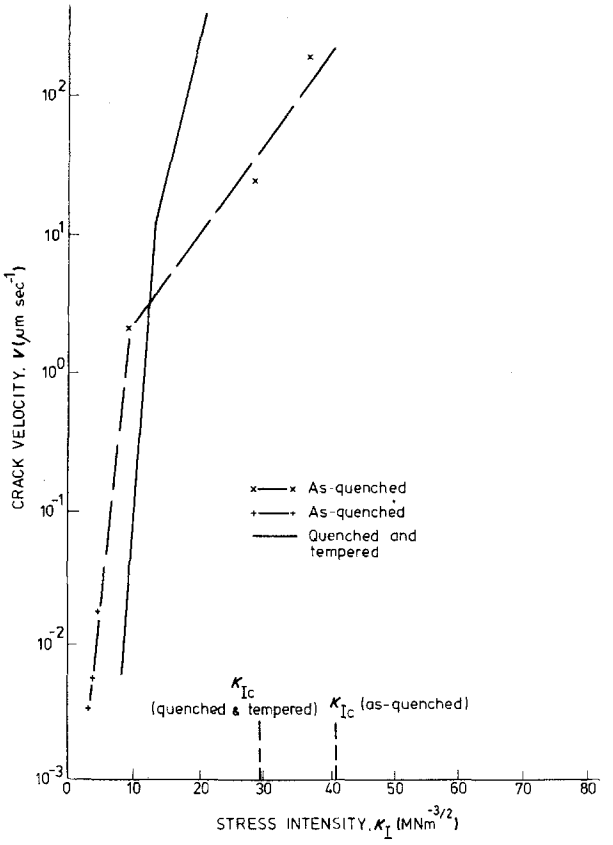

Figure 5 $K-V$ diagrams of AISI 4140 steel obtained in distilled water for the as-quenched and quenched and tempered conditions.

to atomic concentrations from a knowledge of the relative elemental Auger electron sensitivities, as discussed in a previous publication [31]. The sensitivity ratios used in the present study are 2.07, 1.60 and 1.12 for P, N and Ni respectively.

3.6. Mechanical properties/metallography

The critical stress intensity, K_{IC}, was determined by testing the double torsion test pieces to failure under ambient conditions. The resultant fracture surfaces were subsequently examined using scanning electron microscopy with particular attention directed at investigating any changes in the mode of fracture as a function of crack velocity.

To aid the interpretation of the stress corrosion results tensile tests were conducted on specimens exposed to ambient conditions or enclosed in plastic envelopes containing distilled water.

4. Results and discussion

4.1. SCC of as-quenched AISI 4140 in distilled water

Difficulty was experienced, with the as-quenched martensitic material, in inducing a crack to propagate along the V-groove of the specimen. Stress corrosion cracks did form, but usually nucleated at one corner of the rectangular starter notch and propagated away from the groove. This produced continuous changes in stress intensity conditions at the crack tip and the results were therefore discarded. One crack, however, ran approximately parallel to the groove, and in another case the introduction of a sharp V-notch at the end of the rectangular notch did induce a crack to run in the groove. Results from these two specimens are plotted in Fig. 5 where the lower velocity results refer to the first specimen. The as-quenched material exhibited an extremely low K_{th} of 3 MNm$^{-3/2}$ followed by a two-stage $K-V$ curve and a K_{IC} of 41 MNm$^{-3/2}$. In contrast to the conventional $K-V$ dependence (Fig. 1), no stage II was detected in which the crack velocity was independent of K. Possible reasons for the absence of stage II are discussed in Section 5.

A fractographic examination showed that an intergranular fracture mode was present in all areas of the fracture surface, independent of crack velocity. An intergranular fracture mode (Fig. 6) was also produced by impact fracture in the Auger

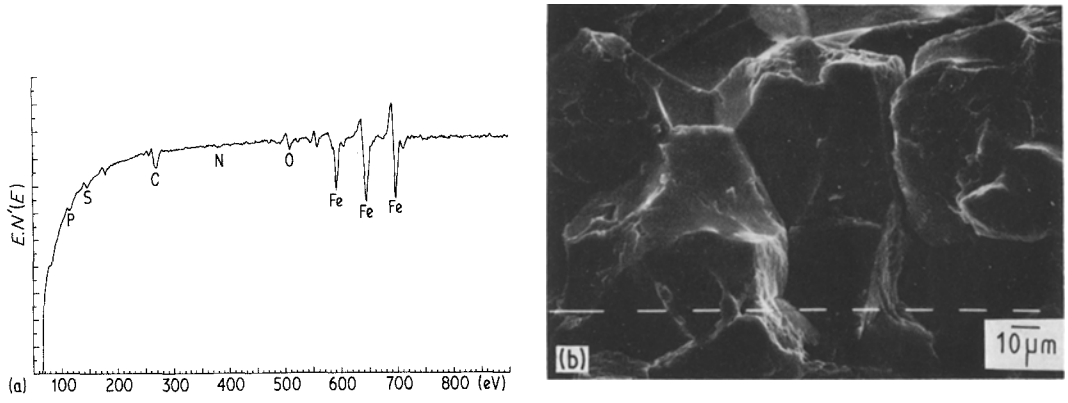

Figure 6 Typical (a) AES spectrum and (b) a micrograph, obtained from the intergranular fracture surface of AISI 4140 steel in the as-quenched state.

spectrometer at ambient temperature. A typical AES spectrum obtained from the fracture surface is shown in Fig. 6 which shows the presence of low levels of phosphorus and nitrogen. Argon ion bombardment showed that this segregation was confined to the first few monolayers of the surface. A quantification of the spectra is presented in Table III. These observations indicate the segregation of both phosphorus and nitrogen to the austenite grain boundaries whilst in the γ-field and this is consistent with previous studies on other alloy steels [26, 32, 33]. It should be noted, however, that the sample was subjected to an 8 h treatment at 150° C during the bake-out of the Auger UHV system and some segregation may possibly have occurred at this stage.

4.2. SCC of tempered AISI 4140 in distilled water

Fig. 7 compares $K-V$ diagrams obtained by optical and load relaxation methods. The former gave good reproducibility of results, as shown by the data from specimens 2 and 6. No crack propagation could be detected when the stress intensity was less than 8 $MNm^{-3/2}$ and this figure was therefore taken as the threshold stress intensity for stress corrosion, and the curve accordingly drawn perpendicular to the stress intensity axis from this point. A two stage $K-V$ curve was obtained, similar to that observed for the as-quenched material (Fig. 5) but with the slope in the second region (stage III) steeper than that for the as-quenched material, together with a lower K_{IC}. Stage III was also much steeper than the corresponding part of the $K-V$ diagram obtained by Brunton [24] for AISI 4140 steel embrittled at the same temperature, using an optical method of measurement. There is close agreement with Brunton, however, in the low crack velocity region, (stage I). Both studies indicate a threshold stress intensity in the range 8 to 12 $MNm^{-3/2}$ for stress corrosion crack growth. This, in the present work, is only one third of the critical stress intensity factor, K_{IC}, which was determined using the same specimens, by testing them rapidly to failure under ambient conditions. The slope of the stage I portion of the $K-V$ diagram was steep; about three orders of magnitude increase in crack velocity for a 5 $MNm^{-3/2}$ increase in K_I. In stage III the slope was reduced to one third of this value.

Results obtained by the load–relaxation method are also plotted in Fig. 7. Stage III crack velocities in specimens 3 and 6 were remarkably close to those measured in specimens 2 and 6 using the optical method. Crack velocities in stage III derived from load–relaxation curves for other specimens,

TABLE III Summary of the AES results obtained from the as-fractured surfaces

Condition	Peak height as a percentage of Fe (703 eV) peak height				Atomic concentration (%)			
	P	N	Sn	Ni	P	N	Sn	Ni
AISI 4140, as-quenched	2.2	1.7	–	–	1.1	1.1	–	–
AISI 4140, tempered, 2 h, 250° C	7.1	1.9	–	–	3.4	1.1	–	–
En30A, tempered, 1 h, 650° C and 24 h, 500° C	20.1	0.7	1.9	13.1	9.7	0.4	3.3	11.7

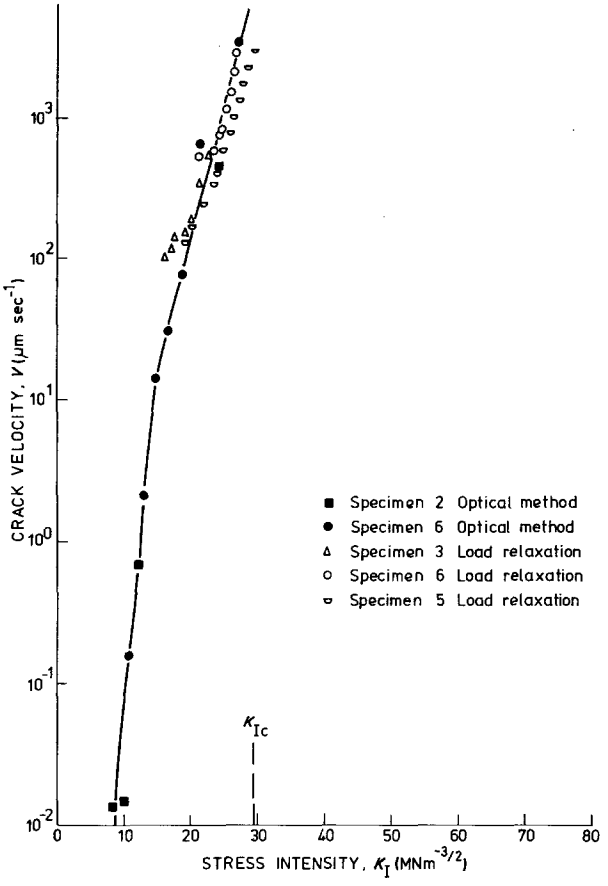

Figure 7 A comparison of the $K-V$ diagrams obtained using the optical and load–relaxation methods for AISI 4140 steel in the tempered condition.

however, were as much as an order of magnitude less, although the slopes of all the curves were similar. Thermal instability of the testing machine during longer term experiments led to spurious changes in the slope of the load–relaxation curve as the load reduced to low levels and made crack velocity determination in stage I by this method almost impossible. The one set of results obtained for this part of the diagram gave a curve with a similar slope to the one obtained by optical measurement, but indicated crack velocities 10^3 times slower for a given stress intensity. Extension of the stage I curve to the stress intensity axis indicates a threshold stress intensity of $\sim 13\,\mathrm{MNm}^{-3/2}$.

Fracture surfaces of specimens which, after stress corrosion experiments, had been broken to determine K_{IC}, were examined in the scanning electron microscope. Irrespective of whether the crack growth was slow (stage I), fast (stage III) or catastrophic (critical), crack propagation was intergranular, along the prior austenite grain boundaries as shown in Fig. 8a to c. In most cases, grain boundary cracking was also observed in boundaries intersecting the fracture surfaces. This, however, was not necessarily a result of stress corrosion, as it was also observed in specimens fractured in the Auger spectrometer, under UHV. AES analyses were made from an array of points over the fracture surface and a typical spectrum obtained is shown in Fig. 9. The results showed that P and N were segregated at the intergranular facets and to within the resolution of the spectrometer (4 μm) an even distribution of segregated species existed across the whole fracture surface. Argon ion bombardment of the fracture surfaces, Fig. 10, showed that P and N were confined to within the first few monolayers of the fracture surface, with the concentration of P at the grain boundary being ~ 180 times that of the bulk (Table III). Similar levels of N were detected at the boundary in the as-quenched and the tempered condition but the P concentration increased significantly on tempering at 250° C. This observation is in conflict with that reported by Banerji *et al.* [26] in 4340 steel.

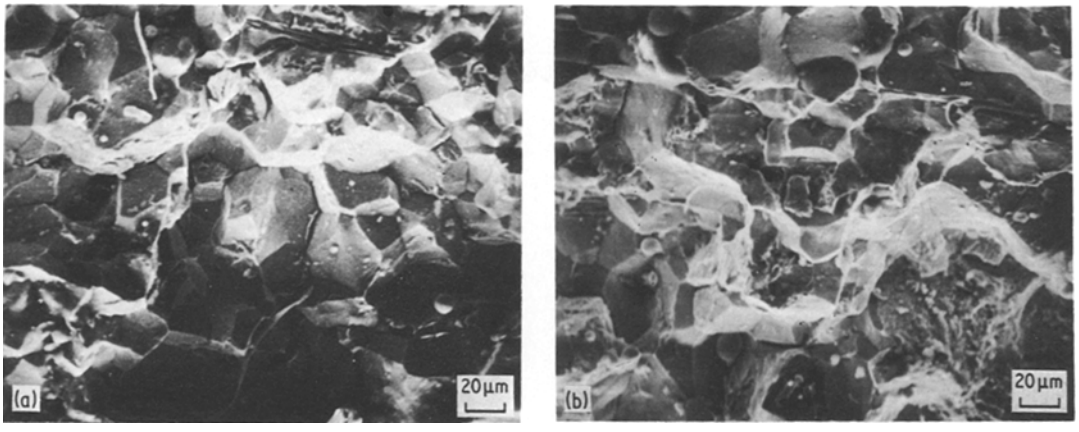

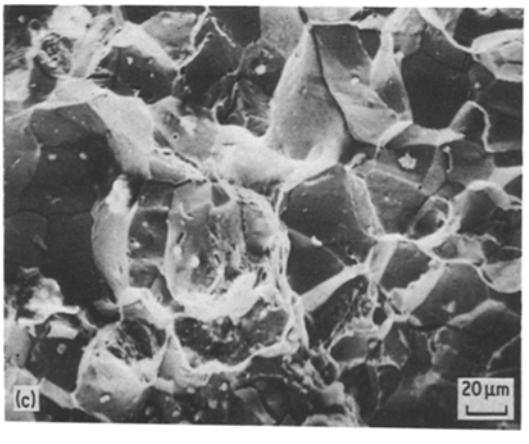

Figure 8 Fractographs obtained from the double torsion test piece of tempered AISI 4140 corresponding to (a) stage I, (b) stage III and (c) catastrophic failure.

4.3. SCC of tempered AISI 4140 steel in ambient air

Fig. 11 compares the $K-V$ diagram for specimen 3 (the same specimen for which load–relaxation results in water had been obtained) in ambient air, obtained by the optical measurement method, with the distilled water results from Fig. 7 obtained by the same method. The air temperature was 19 to 25° C and its relative humidity varied between 42 and 71% during the several days the test was in progress. These were natural room variations which could not be controlled, but appeared to have no significant effect on crack growth rates. The diagram for ambient air conditions is shifted along the stress intensity axis, indicating a much greater threshold intensity, $\sim 21\,MNm^{-3/2}$, for stress corrosion cracking in those conditions. True crack growth rates in air are, however, grossly underestimated in the results of Fig. 11. Microscope observation during these tests revealed that crack growth was not continuous, but occurred by a slip–stick mode. A similar observation was reported by Briant *et al.* [34] for HY 130 steel in gaseous hydrogen. The growth rates during the slip stages were much greater than those suggested by the values averaged over time, (Fig. 11), which include periods of no growth. Transient crack growth rates in ambient air might therefore be as fast as in distilled water, but between spurts of growth the crack is quasi-stable, as though an incubation stage is necessary before the next growth phase can begin.

Attempts to obtain a $K-V$ diagram for AISI 4140 steel in air by the load–relaxation method produced apparent crack velocities 10^6 to 10^7 times slower than the maintained load method. It is assumed that, in the former case, because the load was relaxing, and the driving force therefore reducing, the crack spent even longer periods in the "stick" phase. Fractographic analyses showed that the crack propagated in an intergranular manner in all the stages of the $K-V$ curve. It is possible that slip–stick growth occurred also in the distilled water environment but, if so, it was on such a fine scale, with incubation times between spurts so short, that observation of that mode of growth was not possible. Under the microscope growth appeared continuous.

4.4. SCC of unembrittled En30A steel in distilled water

Stress corrosion cracks were initiated by application of 1000 kg load, corresponding to a stress intensity of $100\,MNm^{-3/2}$, and could be grown a few millimetres into the specimens. At lower stress

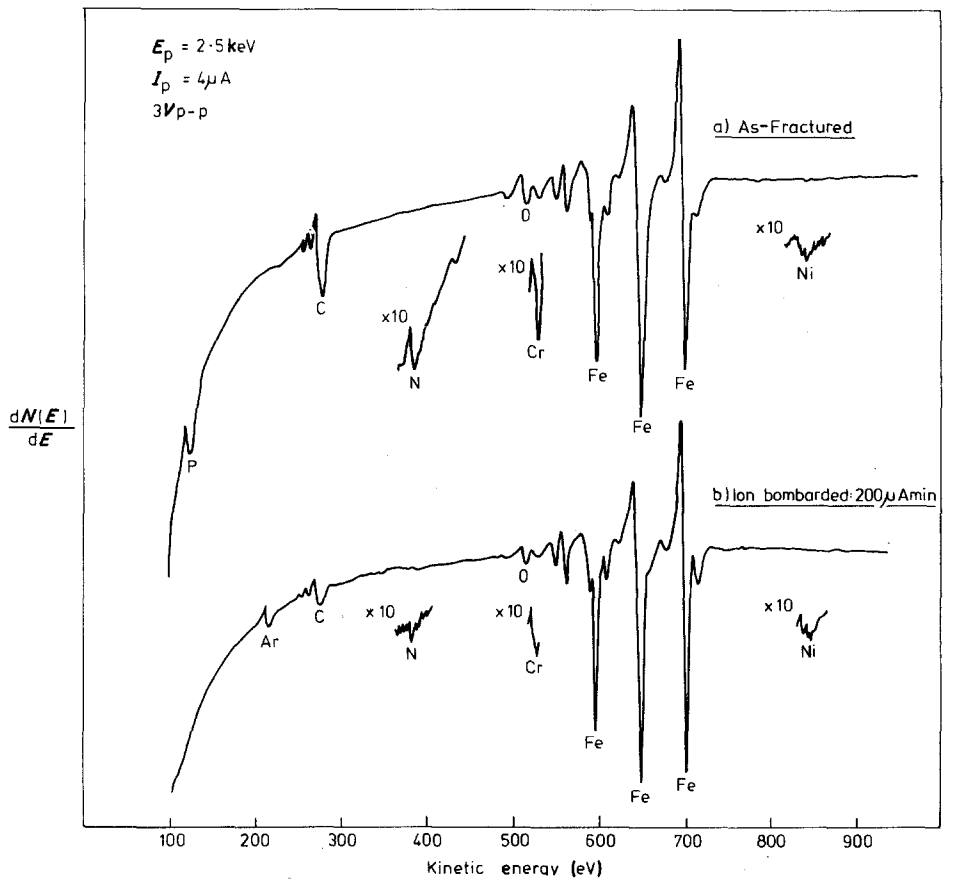

Figure 9 (a) AES spectrum of the as-fractured intergranular surface of AISI 4140 steel in the tempered state. (b) AES spectrum obtained from the fracture surface after an argon ion bombardment of 200 μA min.

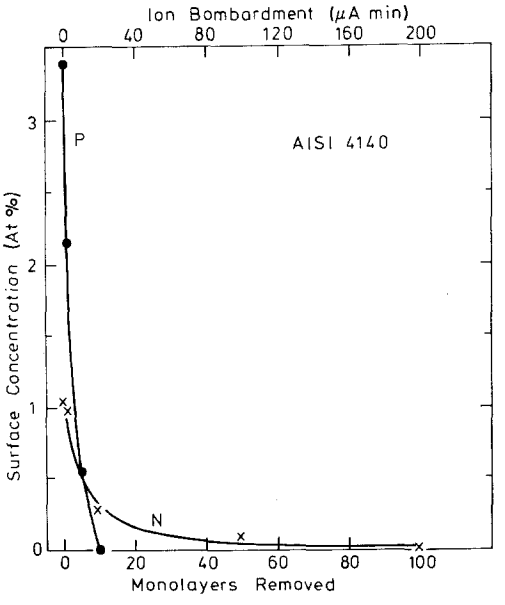

Figure 10 Distribution of the trace impurities phosphorus and nitrogen as a function of distance from the fracture surface in tempered AISI 4140.

intensities no growth could be detected, whilst greater stress intensities at first produced faster growth, but then substantial plastic deformation occurred and prevented further crack growth. Some crack velocities were obtained from optical measurements, but the results were highly variable and could not be presented in the form of a $K-V$ diagram. In these experiments the specimens were so severely bent that they began to foul the bottom of the water container surrounding the loading jig. Because of the plastic deformation, no K_{IC} value could be determined for the steel in this condition, even when the specimens were cooled with liquid nitrogen.

4.5. SCC of temper embrittled En30A steel in distilled water

Preliminary experiments using the load–relaxation method, with specimens immersed in water at 20° C, were unsuccessful in that spalling of surface material around the load location holes gave rise to spurious load relaxations, but no crack growth was

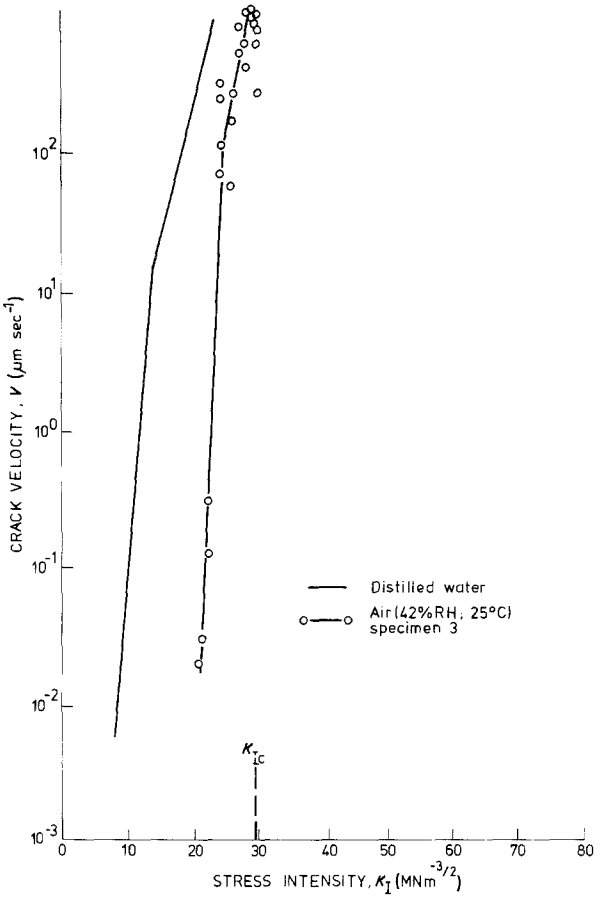

Figure 11 $K-V$ diagrams obtained in distilled water and ambient air for AISI 4140 steel in the tempered condition.

detected. Similar spalling also occurred around the starter notch. The spalling, shown in Fig. 12, indicates the existence of an embrittled surface layer. A second specimen also spalled, but in spite of this it was used to show that stress corrosion could occur in the material, and two optical method measurements of crack growth rate were obtained. They are shown in the $K-V$ diagram of Fig. 13. General corrosion of the surface of this specimen made location of the crack tip difficult, and therefore crack velocities corresponding to lower stress intensities were impossible to determine. However, in an attempt to reduce the incidence of spalling, tests were carried out at

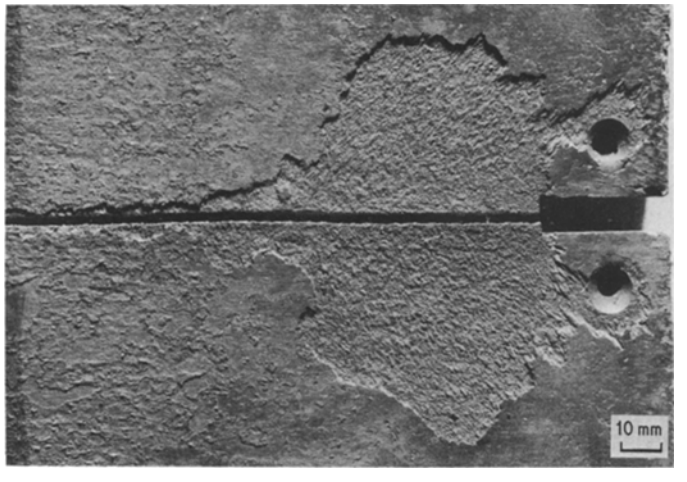

Figure 12 Spalling of the test piece observed around the starter notch in En30A in the temper-embrittled condition.

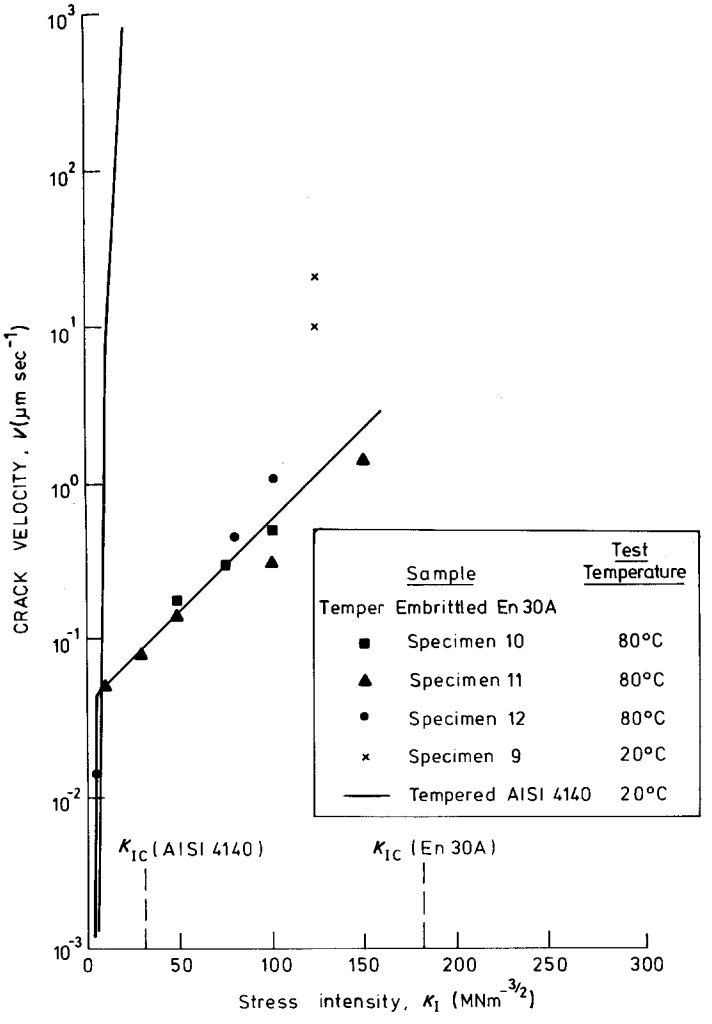

Figure 13 $K-V$ diagram obtained in distilled water (at 80° C) for En30A steel in the temper-embrittled condition.

higher temperatures. It was found that, in water at 80° C, little spalling occurred, and corrosion products were more easily removed to reveal the crack position. Reproducible results were obtained from three specimens, and they are presented in Fig. 13. Most of the data points appear to lie on stage III of the $K-V$ diagram; only one indicating the existence of a stage I curve, and implying a very low threshold stress intensity for En30A ($\sim 5\,\mathrm{MNm}^{-3/2}$). Critical stress intensities were determined for two of these specimens by rapid testing to failure in air after data for stress corrosion in water had been obtained. K_{IC} values for En30A given in Fig. 13 were much greater than those for AISI 4140. During these tests the specimens suffered substantial permanent deformation.

Examination of the fracture surfaces in the scanning electron microscope showed that, during stress corrosion and during the fast fracture of the K_{IC} determinations, crack propagation was totally intergranular.

An intergranular fracture mode was obtained on fracturing *in situ* at low temperature in the Auger spectrometer and a typical AES spectrum obtained is shown in Fig. 14. Segregation of Sn, P, N and Ni was noted, in agreement with a parallel study on the temper embrittlement behaviour of En30A [35]. A quantification of the spectra is shown in Table III. The observed segregation of both the major alloying element, nickel, and the trace impurities, phosphorus and tin, is typical of a temper embrittled steel. Argon ion bombardment established that the trace impurities were confined to within the first few monolayers of the fracture surface, whereas the concentration of nickel approached the bulk concentration over ~ 100 atomic layers.

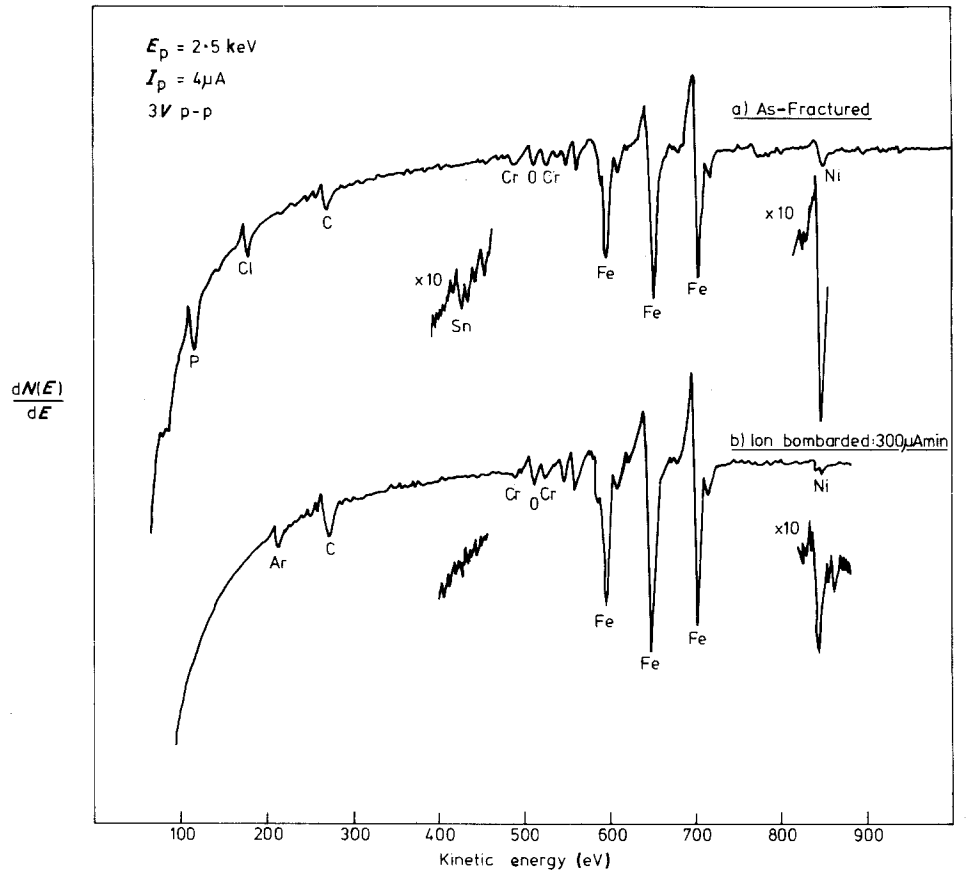

Figure 14 (a) AES spectrum obtained from the intergranular fracture surface of En30A in the temper-embrittled condition. (b) AES spectrum obtained from the intergranular fracture surface after an ion bombardment of 300 μA min, corresponding to a surface removal of ~ 150 atomic layers.

4.6. Mechanical tensile testing

Brown and Srawley [36] proposed a figure of merit for materials susceptible to stress corrosion cracking, which related the threshold stress intensity, K_{ISCC} or K_{th}, and the yield point σ_y, to a critical flaw depth, a_{cr}, through the following equation

$$a_{cr} = 0.2\left(\frac{K_{ISCC}}{\sigma_y}\right)^2. \quad (7)$$

In the present work tensile tests were carried out on small, dumb-bell shaped, specimens (rectangular or circular cross-section) machined from broken stress corrosion plates. Two to five specimens of AISI 4140 in the quenched or tempered condition and En30A in the embrittled condition were tested in air or distilled water. The results, which showed negligible scatter, are presented in Table IV, which also gives K_{ISCC} and the derived figure of merit, a_{cr}. The implication from the very small values of the latter is that stress corrosion cracking would be expected to occur in any structure made from these steels and subjected to the appropriate temperatures, stress intensities and environments.

TABLE IV Yield strength, threshold stress intensity and figure of merit of the conditions studied

Steel	Heat treatment	Environment	Yield strength (MNm^{-2})	K_{ISCC} ($MNm^{-3/2}$)	a_{cr} (μm)
AISI 4140	Quenched	Water	1430	3	1
		Air	1430	–	–
AISI 4140	Quenched and tempered	Water	1370	8	7
		Air	1370	21	47
En30A	Quenched and embrittled	Water	765	4	5.5
		Air	765	–	–

5. General discussion

5.1. Intergranular failure

A common feature of the AISI 4140 samples examined was the intergranular nature of the fracture. This was not simply a result of testing in aggressive environments as the same mode of fracture was also produced in UHV.

Lui and May [27] reported intergranular fracture of AISI 4140 in the as-quenched and quenched and tempered (at $\sim 200^\circ$ C) conditions in fatigue testing. Samples tempered at high temperatures ($> 300^\circ$ C) failed in a transgranular manner. A double etching technique [37] was used for the preparation of carbide extraction replicas and it was shown that the incidence of intergranular fracture was concomitant with the presence of thin carbide platelets at the grain boundaries. These films were superseded by discrete carbide particles at higher tempering temperatures ($> 300^\circ$ C), which corresponded with the change to transgranular fracture. It was postulated [27] that the thin carbide platelets were effective barriers to dislocation motion resulting in dislocation pile-ups and subsequent decohesion of the boundaries.

In the present study, AES has demonstrated the grain boundary segregation of phosphorus and nitrogen in both the as-quenched and quenched tempered states. This grain boundary segregation is an important factor not previously appreciated in AISI 4140 and it is considered that it plays the dominant role in promoting intergranular failure, with the type and morphology of the carbide(s) having a secondary influence. As discussed later, it is considered that this segregation also exacerbates the susceptibility to stress corrosion cracking.

The low alloy Ni–Cr steel, En30A, was tested at a lower strength level than the AISI 4140, in both an unembrittled and temper-embrittled state. Intergranular fracture was obtained in the temper-embrittled condition and was shown to be promoted by the grain boundary segregation of the major alloying element, nickel and the trace impurities, tin and phosphorus. In contrast, the unembrittled material was shown to exhibit a transgranular ductile fracture.

5.2. $K-V$ diagrams

The profile of the crack front produced using the double torsion test is shown in Fig. 15. The crack front extended further along the tension than along the compression face of the specimen, and was curved along most of its length, but entered the tension face orthogonally, as shown in Fig. 15. This is a photograph of matching fracture faces placed side by side, and shows the positions of the crack front after two successive stress corrosion experiments. The crack moved from left to right, and its orthogonal approach to the tension surface can be seen particularly well in its first stopping position. As pointed out by Williams and Evans [3], this implies that plane stress conditions exist at the leading edge of the crack. No geometrical correction for the crack velocity is therefore necessary.

A significant feature of the $K-V$ diagrams obtained for AISI 4140 and En30A was the absence of stage II behaviour (Fig. 1) in which the crack velocity is independent of K value. Norontia and Packman [38] have suggested that the insensitivity to K value generally observed in stage II is a result of crack blunting which lowers the effective stress intensity. The computation for K is normally based on a sharp crack tip geometry and any crack micro-branching resulting in blunting renders the elastic fracture mechanics computation invalid.

It is postulated that, in the present tests, a two stage curve is produced because of no effective crack blunting during crack propagation and the crack velocity is not limited by the rate of diffusion of hydrogen to the crack tip. Stage I reflects the reaction rate at the crack tip/environment interface and stage III is controlled by the rate of reaction between the liberated hydrogen

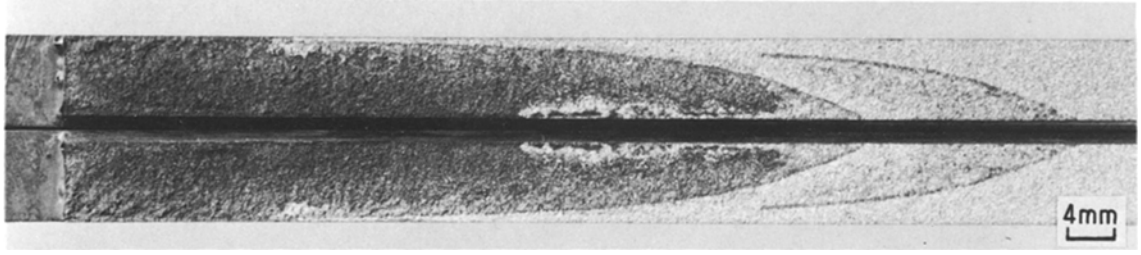

Figure 15 Fracture surfaces of double torsion test piece illustrating crack front geometry.

and the material ahead of the crack tip. In the case of intergranular fracture the susceptibility to hydrogen-assisted cracking is exacerbated by the grain boundary segregation of trace impurities. The dependence of this interaction on the level of segregated species is illustrated in Fig. 5. Tempering at 250° C produces an increase in the grain boundary segregation of phosphorus from 1.1 to 3.4 at% together with a decrease in ultimate tensile strength (UTS) and an approximately constant yield stress. This increase in the grain boundary segregation produces an increase in the slope of stage III indicating a greater reduction in the grain boundary cohesive strength together with a decrease in K_{IC} from 41 to 31 $MNm^{-3/2}$.

An interesting feature of the $K-V$ curves of the as-quenched AISI 4140 material is the extremely low value of K_{th}, which is lower than that of the more highly segregated tempered material. This anomalous behaviour may be explained as a result of the presence of high residual stresses, produced by the phase transformation which occurs during quenching. Such an explanation has also been presented to explain the low fatigue limit observed in as-quenched material [27]. These residual stresses are tensile in nature and are thus additive to the applied tensile stress resulting in a higher "effective" stress acting on the sample. The apparent K_I computed for the double torsion test is therefore lower than the "effective" K_I acting at the crack tip.

In the cases of as-quenched or temper-embrittled AISI 4140 steel tested in distilled water, the double torsion test gave satisfactory and reproducible results in all stages of the $K-V$ diagram when the optical crack-monitoring method was used. The load–relaxation results for embrittled AISI 4140, however, whilst similar to the optical monitoring results for some specimens, indicated crack velocities varying over an order of magnitude in the high stress intensity part of the $K-V$ diagram. For lower stress intensities, corresponding to stage I of the diagram, results were difficult to obtain by this method, because the slope of the load–relaxation curve had become so small that it could be influenced by thermal instability of the testing machine caused by room temperature variations.

The applicability of the double torsion test to tougher steels was assessed using En30A in an unembrittled and temper-embrittled state. The 1 h at 650° C treatment produced a considerably lower strength level than that of the AISI 4140 conditions studied and temper embrittlement was subsequently induced on ageing at 500° C. The steel in a temper-embrittled condition failed in an intergranular manner on testing in distilled water and $K-V$ diagrams were obtained. In contrast no $K-V$ dependence could be determined for the unembrittled state due to extensive plastic deformation at the crack tip.

6. Conclusions

1. The segregation of trace impurities to the prior austenite grain boundaries greatly exacerbated the susceptibility to stress corrosion cracking of AISI 4140 and En30A steels.

(a) Phosphorus and nitrogen segregation was observed in AISI 4140 in the as-quenched condition, with the phosphorus level increasing on tempering at 250° C. This segregation lowered the cohesive strength of the grain boundaries and promoted an intergranular fracture mode both in UHV and in aggressive environments. The increase in the phosphorus concentration at 250° C decreased K_{IC} and increased the slope of stage III in the $K-V$ curve. An anomalously low K_{th} was observed in the as-quenched material which was attributed to the presence of residual tensile stresses. This resulted in the effective K acting on the sample being greater than K calculated from the applied load. Testing in air resulted in an increase in the K_{th} obtained in distilled water.

(b) The temper embrittlement treatment of En30A produced the grain boundary segregation of Ni, Sn and P, resulting in a reduction in the cohesive strength of the grain boundaries and the promotion of intergranular fracture. The limited data obtained indicated an even lower K_{th} for embrittled En30A than for tempered AISI 4140. In unembrittled En30A useful crack velocity measurements could not be made because of the crack blunting effects of plastic deformation.

2. Stress corrosion cracking occurred in tempered AISI 4140 in ambient air by a "slip–stick" mechanism which precluded the measurement of true crack velocities. K_{th} in these conditions was much greater than in distilled water (22 $MNm^{-3/2}$ compared with 8 $MNm^{-3/2}$) and an incubation stage appeared to be necessary between spurts of crack growth.

3. The double torsion fracture mechanics test could be used satisfactorily with AISI 4140 steel in as-quenched and tempered conditions, and

with En30A steel in the temper-embrittled condition. An optical crack monitoring method was capable of giving more reproducible results, covering a wider range of crack velocities, than a load–relaxation method in the absence of elaborate precautions to prevent thermal instability of the testing equipment.

References

1. J. O. OUTWATER and D. J. GERRY, *Mod. Plast.*, Oct. (1967).
2. G. HANCOCK and H. H. JOHNSON, *Trans. Met. Soc. AIME* **236** (1966) 513.
3. D. P. WILLIAMS and A. G. EVANS, *J. Test. Eval.* **1** (1973) 264.
4. A. V. VIRKAR and R. S. GORDON, *J. Amer. Ceram. Soc.* **59** (1976) 68.
5. "Stress Corrosion Cracking and Hydrogen Embrittlement of Iron Base Alloys", edited by R. W. Staehle, J. Hockman, H. E. Slater and R. D. McCright, (National Association of Corrosion Engineers, Houston, 1976).
6. T. G. MCCORD, B. W. BUSSERT, R. M. CURRAN and G. C. GOULD, *Mater. Performance* **15** (1976) 25.
7. F. J. NORTON, *J. Appl. Phys.* **11** (1940) 262.
8. R. C. FRANK and D. E. SWETS, *ibid.* **28** (1957) 380.
9. B. F. BROWN, Naval Research Laboratory *Report 6041* (1963).
10. E. H. PHELPS, Proceedings of the Conference on the Fundamental Aspects of Stress Corrosion Cracking, Ohio State University, September, 1967, (National Association of Corrosion Engineers, Houston, 1969) p. 398.
11. H. H. UHLIG, *Met. Prog.* **57** (1950) 486.
12. H. H. JOHNSON and A. M. WILMER, *Appl. Mater. Res.* **14** (1965) 34.
13. J. A. SMITH, M. H. PETERSON and B. F. BROWN, *Corrosion* **26** (1970) 539.
14. H. W. HAYDEN and S. FLOREEN, *ibid.* **27** (1971) 429.
15. D. P. DAUTOVICH and S. FLOREEN, *Met. Trans.* **4** (1973) 2627.
16. C. ST. JOHN and W. W. GERBERICH, *ibid.* **4** (1973) 598.
17. B. F. BROWN in "The Theory of Stress Corrosion Cracking in Alloys", edited by J. C. Scully (NATO Scientific Affairs Division, Brussels, 1971) p. 186.
18. B. F. BROWN, *Metall. Rev.* **13** (1968) 171.
19. J. O. OUTWATER, M. C. MURPHY, R. G. KUMBLE and J. T. BERRY, *ASTM STP* **559** (1974).
20. A. G. EVANS, *J. Mater. Sci.* **7** (1972) 1137.
21. D. P. WILLIAMS and A. G. EVANS, *J. Test. Eval.* **1** (1973) 264.
22. A. G. EVANS, *Int. J. Fract.* **9** (1973) 267.
23. J. A. KIES and A. B. J. CLARK, in "Fracture 1969," edited by P. L. Pratt (Chapman and Hall, London, 1969) p. 483.
24. J. H. BRUNTON, *CUED/C-MAT/TR*, (1973).
25. K. YOSHINO and C. J. MCMAHON Jr, *Met. Trans.* **5** (1974) 363.
26. S. K. BANERJI, C. J. MCMAHON Jr and H. C. FENG, *ibid.* **9A** (1978) 237.
27. H. W. LUI and I. LE MAY, "Grain Boundaries in Engineering Materials" in Proceedings of the 4th Bolton Landing Conference, 1974, edited by J. L. Walter, J. H. Westbrook and D. A. Woodford (Publishing Division, Baton Rouge, 1975) p. 397.
28. S. DINDA and W. R. WARKE, *Mater. Sci. Eng.* **24** (1976) 199.
29. J. P. COAD, J. C. RIVIÈRE, M. GUTTMANN and P. R. KRAHE, AERE R-8355 (1976).
30. R. E. WEBER and A. L. JOHNSON, *J. Appl. Phys.* **40** (1969) 314.
31. B. C. EDWARDS, H. E. BISHOP, J. C. RIVIÈRE and B. L. EYRE, *Acta. Metall.* **24** (1976) 957.
32. B. J. SCHULTZ and C. J. MCMAHON Jr, "Temper Embrittlement of Alloy Steels", *ASTM STP 499* (Amer. Soc. Test. Mater., 1972) p. 104.
33. B. C. EDWARDS, M. NASIM and E. A. WILSON, *Scripta Metall.* **12** (1978) 377.
34. C. L. BRIANT, H. C. FENG and C. J. MCMAHON Jr, *Met. Trans.* **9A** (1978) 625.
35. B. C. EDWARDS, B. L. EYRE and G. GAGE, *Acta. Metall.* **28** (1980) 335.
36. W. F. BROWN and J. E. SRAWLEY, "Plane Strain Crack Toughness Testing of High Strength Metallic Materials", *ASTM STP 410* (Amer. Soc. Test. Mater., 1966).
37. M. W. LUI and I. LE MAY, "Microstructural Science", Vol. 2 (American Elsevier, New York, 1974) p. 35.
38. P. J. NORONTIA and P. F. PACKMAN, *Eng. Fract. Mech.* **10** (1978) 289.

Received 22 May and accepted 13 June 1980.